

# ClinKD: Cross-Modal Clinical Knowledge Distiller For Multi-Task Medical Images

Hongyu Ge<sup>1</sup> Longkun Hao<sup>1\*</sup> Zihui Xu<sup>1\*</sup> Zhenxin Lin<sup>2</sup> Bin Li<sup>3†</sup> Shoujun Zhou<sup>3†</sup>  
 Hongjin Zhao<sup>4</sup> Yihang Liu<sup>1</sup>

<sup>1</sup> Shandong University

<sup>2</sup> Hubei University

<sup>3</sup> Shenzhen Institutes of Advanced Technology, Chinese Academy of Sciences

<sup>4</sup> Australian National University

## Abstract

Medical Visual Question Answering (Med-VQA) represents a critical and challenging subtask within the general VQA domain. Despite significant advancements in general Visual Question Answering (VQA), multimodal large language models (MLLMs) still exhibit substantial limitations when handling multi-task VQA scenarios. These limitations manifest through erroneous spatial localization and misinterpretation of medical images, which primarily arise from two fundamental issues: inadequate image-text alignment and insufficient medical knowledge in general-purpose MLLMs for specialized medical applications. To address these issues, we introduce the Cross-Modal **Clinical Knowledge Distiller (ClinKD)**, an innovative framework designed to enhance image-text alignment and establish more effective medical knowledge adaptation mechanisms, which enables MLLMs to adapt to medical knowledge. Our extensive experimental evaluations demonstrate that the ClinKD achieves state-of-the-art performance on the Med-GRIT-270k dataset, a challenging medical benchmark containing fine-grained multi-task QA pairs. The results indicate that our approach not only significantly improves image-text alignment but also effectively enables MLLMs to adapt to the medical knowledge. The source code for ClinKD is available at: <https://github.com/overloadedHenry/ClinKD>.

## 1. Introduction

Medical Visual Question Answering (Med-VQA) [1, 10, 25] is a critical domain for applying MLLMs [4, 21, 37] to medical image analysis [19]. Recent advancements in MLLMs have enabled them to achieve preliminary capa-

\*Equal contributions in no particular order.

†Corresponding Authors; Emails: {b.li2, sj.zhou}@siat.ac.cn

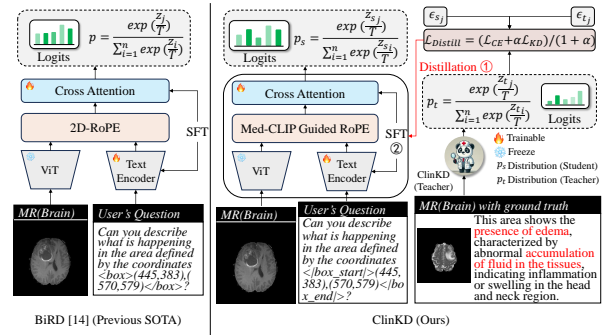


Figure 1. The left part shows that the BiRD [14] only utilizes traditional supervised fine-tuning (SFT) and 2D-RoPE [32] to obtain the capabilities of understanding and grounding medical images. The right part is our method which uses Med-CLIP Guided RoPE for enhancing image-text alignment and Pseudo-Labels Medical Knowledge Distillation for filling the gap of medical knowledge in ClinKD. During the SFT procedure, we will use Reflective Correction Training to enable answers with low semantic similarity or incorrect groundings to be reused.

bilities in image analysis, annotation, and user instruction compliance [5]. Previous studies have made multiple attempts [11, 14, 15, 18, 29, 38] to enhance the performance of general-purpose MLLMs in Med-VQA.

For instance, LLaVA-Med [18] extends instruction-tuning techniques for MLLMs to the medical domain. This work applied instruction tuning and curated image-text datasets to align visual-textual features in LLaVA [27], enabling LLaVA-Med to recognize and analyze medical images. However, this system lacked fine-grained image understanding, causing erroneous spatial localization when questioned about specific pathological locations [9, 14].

Subsequently, the BiRD [14], a model that incorporated fine-grained image recognition by developing a biomedical refer-and-ground instruction-tuning dataset, addresses the

absence of grounding capabilities [40, 42] in LLaVA-Med’s work [18]. Nevertheless, as shown in Figure 1, due to its reliance on traditional supervised fine-tuning (instruction-tuning) [17, 28, 45] and conventional 2D Rotary Position Embedding (RoPE) [32], BiRD tends to generate erroneous spatial localization and misinterpretation of medical images because of incomplete image-text alignment [35, 43]. Moreover, the visual encoder of BiRD is constrained by the lack of medical knowledge, resulting in difficulties in medical knowledge adaptation [24, 47].

To overcome these limitations, we propose a medical distillation framework named ClinKD to boost capabilities in the Med-VQA domain. Specifically, our method mainly focuses on two issues: incomplete image-text alignment and the professional medical knowledge gap between the general-purpose MLLMs and medical domain that requires finer-grained medical knowledge [22, 41].

For the first issue, we propose Med-CLIP Guided Rotary Position Embedding (MCG-RoPE), a novel position embedding method that focuses on the inter-modal and intra-modal intervals during joint image-text training, while ensuring the equivalence of context intervals immediately adjacent to images. Compared to traditional RoPE [32], the MCG-RoPE uses the distinct index intervals to better capture cross-modal information, thereby achieving more effective image-text alignment.

For the second issue, we propose **Clinical Knowledge Distiller (ClinKD)** which consists of Pseudo-Labels Medical Knowledge Distillation and Reflective Correction Training. Pseudo-Labels Medical Knowledge Distillation provides prior medical knowledge by using pseudo-labels [6, 20], filling the gap of prior medical knowledge so that the model can better adapt to medical knowledge during the supervised fine-tuning. Reflective Correction Training allows samples with low semantic similarity to be sent for training again after being enhanced by MLLMs.

Our contributions are summarized as follows:

- We introduce the ClinKD, an innovative distiller designed to establish more effective medical knowledge adaptation mechanisms.
- For solving incomplete image-text alignment, we propose the Med-CLIP Guided Rotary Position Embedding (MCG-RoPE). The MCG-RoPE utilizes the distinct inter-modal and intra-modal features to improve image-text alignment.
- For bridging medical knowledge gap between general-purpose MLLMs and specialized medical applications, we propose the Pseudo-Labels Medical Knowledge Distillation, filling the medical knowledge gap before supervised fine-tuning.
- Extensive experimental results show that the proposed ClinKD achieves the best performance on Med-GRIT-270k [14].

## 2. Related Work

### 2.1. Biomedical Instruction-Tuning Datasets

Many Med-VQA datasets such as VQA-RAD [16] and SLAKE [26] contain only medical images and simple QA pairs. Specifically, these QA pairs do not have the fine-grained descriptions of pathological features. This limitation constrains the ability of MLLMs to perform accurate spatial localization. To boost and evaluate MLLMs’ capabilities in the Med-VQA domain, many biomedical instruction-tuning datasets are designed.

For example, the LLaVA-Med-qa0.2k [46] contains 50 medical images sampled from several modalities such as CT, Angiography and PET and 193 questions according to these medical images. The medical QA pairs are generated by GPT-4 based on the metadata. This dataset is designed to evaluate the capabilities of describing medical images, specifically the biomedical features.

Unlike the LLaVA-Med-qa0.2k [46], the Med-GRIT-270k [14] includes multi-task fine-grained medical QA pairs especially for grounding spatial locations. It is designed to enhance the model’s capabilities in referring and grounding. This multi-task dataset comprises four distinct tasks: Visual Grounding (VG), Referring Object Classification (ROC), Referring Captioning (RC), and Medical Image Analysis (MIA). The VG task evaluates the model’s capability of accurately matching text descriptions to corresponding image regions. The RC task assesses the model’s capability to recognize specific image areas and generate descriptive captions for them. The ROC task examines the model’s understanding of textual information related to particular image regions and their associated visual details. The MIA task evaluates the model’s comprehension of medical images and their multi-modal context. All data is sourced from eight modalities: CT, MR, X-ray, PET, Endoscopy, Dermoscopy, Fundus, and Ultrasound. Utilizing data from these eight modalities allows for a more comprehensive evaluation of the model’s capabilities.

### 2.2. Multimodal Large Language Models (MLLMs) for Biomedicine

With the development of MLLMs, an increasing number of approaches have been applied to the medical field, such as BioMedGPT [44], LLaVA-Med [18], and BiRD [14]. These methods drive the development of MLLMs in the biomedical domain from different perspectives. For instance, LLaVA-Med [18] applied instruction fine-tuning to the medical imaging field and built a medical question-answering system based on LLaVA [27], which provided reasonable responses by processing user-submitted images and instructions. However, LLaVA-Med did not support fine-grained interactions with medical images, meaning that the system cannot precisely locate pathological regions

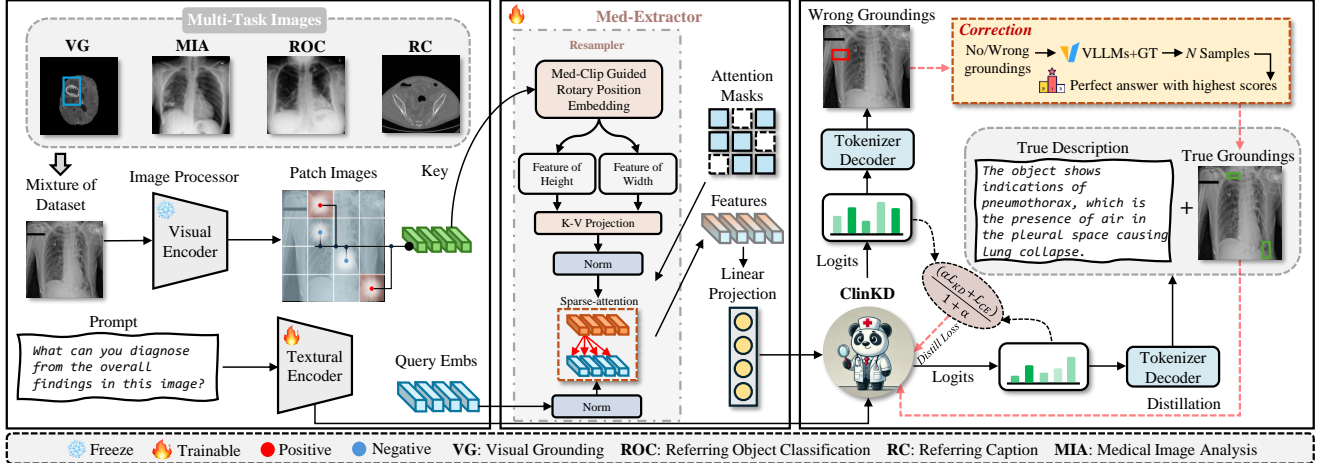


Figure 2. Overview of our ClinKD’s framework: The framework begins with multi-task medical images being segmented into patches. The med-extractor module with Med-CLIP Guided Rotary Position Embedding extracts dimensional features from the patched image embeddings. The ClinKD system undergoes distillation before supervised fine-tuning (SFT). During the SFT, answers with low semantic similarity or incorrect groundings are prioritized for retraining. When responding to queries, the framework selects the answer with the highest score, ensuring accurate medical image analysis and interpretation.

within the images. To address the lack of referring and grounding capabilities, the BiRD [14], which is based on Qwen-VL [3], leveraged a finer-grained medical dataset. However, the ViT of BiRD was not trained by sufficient medical data before being frozen, resulting in a gap in medical knowledge domain. Compared with their work [14, 18], our method modifies the position embedding method and introduces an effective pseudo-labels medical knowledge distillation framework.

### 2.3. Rotary Position Embedding (RoPE)

The introduced RoPE [32] makes the relative position features of the context in the text more easily captured by LLMs. Further, the RoPE-Mixed [12] introduced mixed learnable frequencies to RoPE, enabling it to handle diagonal directions and making RoPE itself learnable. It showed more efficiency when dealing with diagonal features of the image. The VideoRoPE [36] extended the diagonal layout and variable frequency to the video domain, demonstrating its advantages in video analysis tasks. Unlike existing methods, our approach focuses on 2D multi-task medical images where capturing semantic information is challenging. We utilize cross-modal intervals to enable the model to better distinguish modal information, thereby improving image-text alignment.

## 3. Methodology

As shown in Figure 2, we aim at enhancing the ClinKD’s performance by mainly leveraging Med-CLIP Guided Rotary Position Embedding, Pseudo-Labels Medical Knowledge Distillation, Reflective Correction Training and

Semantic-Aware Selective Generation. The proposed Med-CLIP Guided Rotary Position uses the distinct inter-modal and intra-modal space to improve image-text alignment. The distiller provides prior medical knowledge to enhance the model’s capability of medical knowledge adaptation. In the inference procedure, the Semantic-Aware Selective Generation will allow the model to choose the answer with the best score.

### 3.1. Med-CLIP Guided Rotary Position Embedding

The 2D Rotary Position Embedding (RoPE) [32] tends to lack attention on cross-modal features, so we propose the Med-CLIP Guided Rotary Position Embedding (MCG-RoPE) to modify rotation angles that are crucial for image-text alignment. Figure 3 shows the example of our method. **Distinct Inter-Modal Intervals.** Suppose we have a sentence-image-sentence position index sequence:

$$S_{idx} = (T_1, T_2 \cdots, T_\ell, V_{\ell+1}, V_{\ell+2}, \cdots, V_{\ell+wh}, T_{\ell+wh+1}, T_{\ell+wh+2}, \cdots, T_{\ell+wh+k}) \quad (1)$$

where  $T_i = (t_i, t_i)$  denotes the 2D position index of text tokens,  $V_i = (v_i^{(1)}, v_i^{(2)})$  denotes the 2D image index.

To distinguish between intra-modal features and inter-modal features, the indexes of image tokens need to be transformed.

$$(v_i^{(1)}, v_i^{(2)}) \xrightarrow{\mathcal{F}} (\alpha_1 v_i^{(1)} + \lambda_1, \alpha_2 v_i^{(2)} + \lambda_2) = \mathcal{V}_i \quad (2)$$

where  $\mathcal{V}_i$  is the position after being scaled and shifted. The  $\lambda_1, \lambda_2, \alpha_1, \alpha_2$  are parameters. The  $\mathcal{F}$  denotes the operator of shifting and scaling.

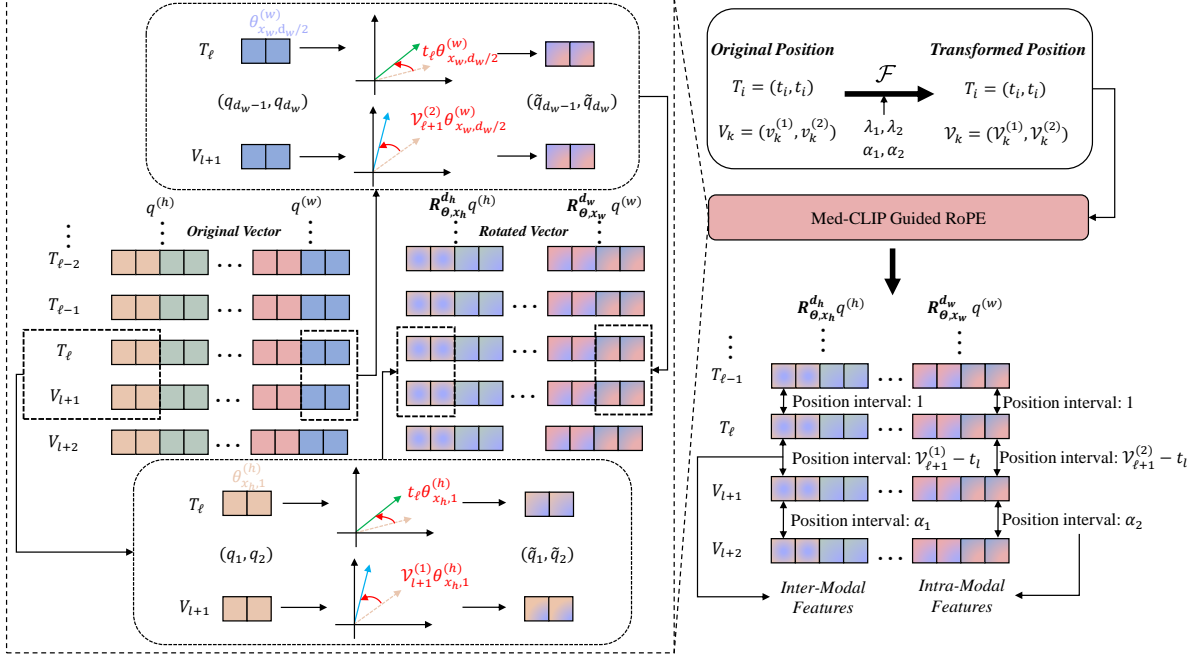


Figure 3. The visualized example of Med-CLIP Guided Rotary Position Embedding. The original vector will be rotated by different angles according to the transformed position indexes. The inter-modal and intra-modal intervals are different so that the Med-CLIP Guided Rotary Position Embedding can better align image feature and text feature.

The inter-modal intervals should be consistent, and thus the following equation needs to be satisfied:

$$\begin{cases} \alpha_1 + \lambda_1 - \ell = \ell + wh + 1 - (\alpha_1 h + \lambda_1) \\ \alpha_2 + \lambda_2 - \ell = \ell + wh + 1 - (\alpha_2 w + \lambda_2) \end{cases} \quad (3)$$

We need to fix  $\alpha_1, \alpha_2$  first to set the intervals between each image's position index. So the general solution is

$$\begin{cases} \lambda_1 = \ell + \frac{wh+1-\alpha_1(h+1)}{2} \\ \lambda_2 = \ell + \frac{wh+1-\alpha_2(w+1)}{2} \end{cases} \quad (4)$$

After setting intervals, the new sequence can be expressed as:

$$\begin{aligned} S_{h-id_x} = & (t_1, \dots, t_\ell, \alpha_1 v_{\ell+1}^{(1)} + \lambda_1, \dots, \\ & \alpha_1 v_{\ell+wh}^{(1)} + \lambda_1, t_{\ell+wh+1}, \dots, t_{\ell+wh+k}) \end{aligned} \quad (5)$$

where  $S_{h-id_x}$  is the position index on height dimension,

$$\begin{aligned} S_{w-id_x} = & (t_1, \dots, t_\ell, \alpha_2 v_{\ell+1}^{(2)} + \lambda_2, \dots, \\ & \alpha_2 v_{\ell+wh}^{(2)} + \lambda_2, t_{\ell+wh+1}, \dots, t_{\ell+wh+k}) \end{aligned} \quad (6)$$

where  $S_{w-id_x}$  is the position index on width dimension.

**Distinct Interval-Based Rotation.** Suppose we have a query/key vector:  $q \in \mathbb{R}^{d_h+d_w}$  where  $\mathbb{R}^{d_h+d_w}$  denotes the  $d_h + d_w$  dimension Euclidean space. The  $d_h, d_w$  denotes

the embedding dimension on height dimension and width dimension respectively. Then  $q$  will be split into  $q^{(h)} \in \mathbb{R}^{d_h}$  and  $q^{(w)} \in \mathbb{R}^{d_w}$

The corresponding frequency on the two dimensions is set as:

$$\begin{aligned} \omega_i^{(h)} &= 10000^{-\frac{2i}{d_h}} \\ \omega_i^{(w)} &= 10000^{-\frac{2i}{d_w}} \end{aligned} \quad (7)$$

Then the angles of rotation are expressed as:

$$\begin{aligned} \theta_{x_h, i}^{(h)} &= x_h \cdot \omega_i^{(h)} \\ \theta_{x_w, i}^{(w)} &= x_w \cdot \omega_i^{(w)} \end{aligned} \quad (8)$$

where  $x_h, x_w$  denote the transformed position index on height and width dimension respectively. This means the angle of rotation will be determined by inter-modal and intra-modal intervals. A large rotation angle brings information of modal transformation while a smaller angle contains fine-grained features of intra-modal. The rotation matrix can be defined as:

$$\begin{aligned} \mathbf{R}_{\Theta, x_h}^{d_h} &= \begin{pmatrix} R_{\theta_{x_h, 1}^{(h)}} & & \\ & \ddots & \\ & & R_{\theta_{x_h, d_h/2}^{(h)}} \end{pmatrix} \\ \mathbf{R}_{\Theta, x_w}^{d_w} &= \begin{pmatrix} R_{\theta_{x_w, 1}^{(w)}} & & \\ & \ddots & \\ & & R_{\theta_{x_w, d_w/2}^{(w)}} \end{pmatrix} \end{aligned} \quad (9)$$

where  $R_{\theta_{x_h,i}^{(h)}}$  and  $R_{\theta_{x_w,i}^{(w)}}$  are defined as:

$$\begin{aligned} R_{\theta_{x_w,i}^{(w)}} &= \begin{pmatrix} \cos \theta_{x_w,i}^{(w)} & -\sin \theta_{x_w,i}^{(w)} \\ \sin \theta_{x_w,i}^{(w)} & \cos \theta_{x_w,i}^{(w)} \end{pmatrix} \\ R_{\theta_{x_h,i}^{(h)}} &= \begin{pmatrix} \cos \theta_{x_h,i}^{(h)} & -\sin \theta_{x_h,i}^{(h)} \\ \sin \theta_{x_h,i}^{(h)} & \cos \theta_{x_h,i}^{(h)} \end{pmatrix} \end{aligned} \quad (10)$$

The rotated vector is shown in Eq. (11):

$$\tilde{q} = \left[ R_{\Theta, x_h}^{d_h} q^{(h)}; R_{\Theta, x_h}^{d_w} q^{(w)} \right] \quad (11)$$

### 3.2. Pseudo-Labels Medical Knowledge Distillation (Pseudo-KD)

Our clinical knowledge distiller enables the student model to learn the output distribution of the teacher model. Therefore, we provide prior knowledge of medical images to the student model through Pseudo-Labels Medical Knowledge Distillation.

The distillation loss function is defined by a linear combination of cross-entropy loss and the Kullback-Leibler Divergence (KL Divergence).

The cross-entropy loss is defined as:

$$\mathcal{L}_{CE} = - \sum_{i=1}^N y_i \log p_s(z_{s_i}) \quad (12)$$

where  $\mathcal{L}_{CE}$  denotes the cross-entropy loss,  $p_s(z_i)$  is the log-its generated by the student ClinKD model and  $y_i$  is the hard label of ground truth.

The KL Divergence mentioned before is defined as:

$$\mathcal{L}_{KD} = T^2 \mathbb{D}_{KL}^{\epsilon_t, \epsilon_s}(p_t \| p_s) \quad (13)$$

where  $\mathcal{L}_{KD}$  denotes the loss function constructed by KL Divergence,  $\mathbb{D}_{KL}^{\epsilon_t, \epsilon_s}(p_t \| p_s)$  is the KL Divergence,  $T$  is called temperature which can smooth the distribution and the  $\epsilon_{s_j}, \epsilon_{t_j}$  are noise values.

Furthermore, the  $\mathbb{D}_{KL}^{\epsilon_t, \epsilon_s}(p_t \| p_s)$  is:

$$\mathbb{D}_{KL}^{\epsilon_t, \epsilon_s}(p_t \| p_s) = \sum_{i=1}^n p_t(z_{t_i} + \epsilon_{t_j}) \log \frac{p_t(z_{t_i} + \epsilon_{t_j})}{p_s(z_{s_i} + \epsilon_{s_j})} \quad (14)$$

where  $p_t(z_i)$  is the probability distribution generated by the teacher ClinKD model,  $p_s(z_i)$  denotes the probability distribution generated by the student ClinKD model.

For details, the distributions are smoothed by temperature  $T$ :

$$\begin{aligned} p_s(z_{s_j} + \epsilon_{s_j}) &= \frac{\exp((z_{s_j} + \epsilon_{s_j})/T)}{\sum_i \exp((z_{s_i} + \epsilon_{s_i})/T)} \\ p_t(z_{t_j} + \epsilon_{t_j}) &= \frac{\exp((z_{t_j} + \epsilon_{t_j})/T)}{\sum_i \exp((z_{t_i} + \epsilon_{t_i})/T)} \end{aligned} \quad (15)$$

Finally the whole distillation loss is expressed as:

$$\mathcal{L}_{Distill} = \frac{\mathcal{L}_{CE} + \alpha \mathcal{L}_{KD}}{1 + \alpha} \quad (16)$$

After obtaining teacher’s prior knowledge about medical images, the student ClinKD model will be trained by supervised fine-tuning (SFT).

### 3.3. Reflective Correction Training

After the model distillation, we restart two rounds of supervised fine-tuning using the whole dataset. During the supervised fine-tuning process, the model’s outputs are recorded and compared with the ground truth. If the semantic similarity between the output and the ground truth falls below 80%, GPT-4o will correct the output based on the ground truth (retaining only the original meaning and anchor box coordinates) to enrich the diversity of the training set labels. The corrected data is then fed back into the training process for further learning.

### 3.4. Semantic-Aware Selective Generation

The responses generated by large language models exhibit randomness, and relying on a single inference may result in missing the optimal answer. Semantic-Aware Selective Generation means that instead of directly using the model’s single-round generation for evaluation, we allow the model to generate multiple samples. We then utilize the CLIP models to score the alignment between the generated text and image. Finally, we reorder the outputs based on these scores and select the one with the highest score as the final result. The pseudo code is shown in Algorithm 1.

---

#### Algorithm 1 Semantic-Aware Selective Generation

---

- 1: **Input:** Image  $I$ , Model  $M$
  - 2: **Output:** Optimal generated text  $T_{final}$
  - 3:  $T_1, T_2, \dots, T_n \leftarrow \text{GenerateSamples}(M, I)$
  - 4: **for**  $i = 1$  **to**  $n$  **do**
  - 5:      $S_i \leftarrow \text{CLIPScore}(T_i, I)$
  - 6: **end for**
  - 7:  $T_{ordered} \leftarrow \text{Sort}(T_1, T_2, \dots, T_n)$
  - 8:  $T_{final} \leftarrow T_{ordered}[1]$
  - 9: **return**  $T_{final}$
- 

## 4. Experiments

### 4.1. Datasets

**Med-GRIT-270k [14].** The Med-GRIT-270k dataset comprises 270k samples, with 240k allocated for training and the remaining 30k for multi-task evaluation. These samples are collected from eight medical modalities: CT, MR, X-ray, PET, Endoscopy, Dermoscopy, Fundus and Ultrasound. Additionally, we randomly select 30K samples



Model	Test dataset	VG (Recall@0.5)	ROC (Recall)	RC (SPICE)	MIA (mBMR)	Average
LLaVA-Med [18]	Med-GRIT-Test30k [7, 39]	0	2.75	8.18	11.20	5.53
BiRD [14]	Med-GRIT-Test30k [7, 39]	53.92	65.33	55.23	52.17	56.66
<b>ClinKD (Ours)</b>	Med-GRIT-Test30k [7, 39]	<b>67.51</b>	<b>82.35</b>	<b>70.56</b>	<b>65.69</b>	<b>71.53</b>
LLaVA-Med [18]	LLaVA-Med-qa0.2k [46]	-	-	-	<b>20.04</b>	-
BiRD [14]	LLaVA-Med-qa0.2k [46]	-	-	-	10.55	-
ClinKD (Ours)	LLaVA-Med-qa0.2k [46]	-	-	-	13.24	-

Table 1. Comparison with LLaVA-Med [18] and BiRD (previous SOTA) [14]. The best scores are shown in bold.

Model	Proposed Methods			VG (Recall@0.5)	ROC (Recall)	RC (SPICE)	MIA (mBMR)	Average
	MCG-RoPE	Pseudo-KD	SASG					
Qwen2-VL [34]	✗	✗	✗	55.43 (+1.51)	68.33 (+3.00)	57.39 (+2.16)	62.23 (+10.06)	61.37 (+4.71)
BiRD [14]	✗	✗	✗	53.92	65.33	55.23	52.17	56.66
	✓	✗	✗	64.03 (+10.11)	72.74 (+7.41)	61.32 (+6.09)	59.63 (+7.46)	64.44 (+7.78)
	✗	✓	✗	66.33 (+12.41)	79.52 (+14.19)	67.21 (+11.98)	64.32 (+12.15)	69.35 (+12.69)
	✗	✗	✓	55.89 (+1.97)	67.84 (+2.51)	54.32 (-0.91)	51.27 (-0.90)	57.33 (+0.67)
<b>ClinKD (Ours)</b>	✓	✓	✓	<b>67.51 (+13.59)</b>	<b>82.35 (+17.02)</b>	<b>70.56 (+15.33)</b>	<b>65.69 (+13.52)</b>	<b>71.53 (+14.87)</b>

Table 2. Ablation study for different models and proposed methods. The value which is blue shows how much the metric scores improved. The best scores are shown in bold. The MCG-RoPE, Pseudo-KD and SASG stand for Med-CLIP Guided RoPE, Pseudo-Labels Medical Knowledge Distillation and Semantic-Aware Selective Generation respectively.

from the entire dataset for pseudo-label generation, which is subsequently used by the Pseudo-Labels Medical Knowledge Distillation. This fine-grained multi-task dataset not only demands that the model accurately understands medical images, but also requires it to precisely classify and ground pathological regions and physiological structures. This poses a significant challenge for MLLMs.

**LLaVA-Med-qa0.2k [46].** The LLaVA-Med-qa0.2k [46] contains 0.2k QA pairs of MIA task which are used for evaluating the models’ ability to analyze medical images. It consists of 50 images with caption pairs and two types of questions: conversation and detailed description.

The images are not only from common modalities such as CT and MR, but also from some modalities that are not available in the Med-GRIT-270k [14] dataset, such as 3D reconstruction. The wide range of data sources evaluates the capabilities of MLLMs in general medical scenarios.

## 4.2. Evaluation Metrics

We use Recall@0.5 for Visual Grounding (VG), Recall for Referring Object Classification (ROC), SPICE [2] for Referring Caption (RC), and mBMR [14] for Medical Image Analysis (MIA). The final overall result is computed as the mean of the evaluation scores across these four tasks.

For the evaluation on LLaVA-Med-qa0.2k [18] which has 0.2k QA pairs of MIA task, we use mBMR as the metric.

## 4.3. Implementation Details

We use Qwen2-VL [34] as the base model for ClinKD. For the Med-CLIP Guided RoPE component of ClinKD, in order to ensure that the position index is an integer, we re-sample the image resolution to  $w = h$ . During the distillation process, we set  $\alpha = 0.5$ ,  $T = 0.5$ . The number of distillation epochs is 2, with an additional 2 epochs for subsequent training. The entire training process is conducted using 6 NVIDIA A100 40G GPUs. The learning rate is set to  $2 \times 10^{-5}$ , and the AdamW optimizer is employed. The learning scheduler follows a cosine schedule. For model generation, we use non-sampling beam search with a beam size of 3.

## 4.4. Analysis

### 4.4.1. Comparison with the State-of-the-Art Methods

**Evaluation on the Med-GRIT-Test30k [7, 39].** As shown in Table 1, we compare ClinKD with BiRD [14] and LLaVA-Med [18]. Results show that ClinKD achieves scores of 67.51%, 82.35%, 70.56%, and 65.69% in the VG, ROC, RC, and MIA tasks respectively, outperforming other comparisons by a clear margin in all tasks. On average, ClinKD outperforms BiRD [14] and LLaVA-Med [18] by 14.87% and 66.00% respectively. ClinKD’s advantages lie in its more adequate image-text alignment and the prior medical knowledge provided by Pseudo-Labels Medical Knowledge Distillation.

**Evaluation on the LLaVA-Med-qa0.2k [46].** Table 1 represents the models’ performance on LLaVA-Med-

Task	Metric	Method	CT	MR	X-ray	PET	Endoscopy	Dermoscopy	Fundus	Ultrasound	Average
VG	Recall@0.5	BiRD [14]	44.47±0.14	29.26±0.11	41.73±0.16	56.46±0.15	53.60±0.12	75.63±0.17	84.15±0.13	46.04±0.18	53.92±0.14
		BiRD [14] + RoPE-Mixed [12]	46.90±0.16	53.11±0.13	42.03±0.17	60.84±0.14	53.49±0.15	78.25±0.11	85.16±0.12	52.83±0.13	59.08±0.19
		BiRD [14] + MCG-RoPE (Ours)	51.22±0.14	49.40±0.18	45.92±0.17	68.60±0.13	60.37±0.19	88.28±0.12	86.59±0.15	61.88±0.16	64.03±0.15
		BiRD [14] + $V_k D$ [30]	58.77±0.12	50.95±0.16	45.69±0.11	65.89±0.18	57.63±0.14	93.32±0.15	79.27±0.12	59.90±0.15	63.93±0.19
		BiRD [14] + Pseudo-KD (Ours)	62.59±0.15	52.86±0.17	47.19±0.13	66.28±0.16	59.84±0.11	93.68±0.18	85.37±0.14	62.87±0.19	66.33±0.13
		ClinKD (Ours)	<b>65.52±0.13</b>	<b>52.23±0.30</b>	<b>48.56±0.19</b>	<b>69.25±0.12</b>	<b>60.37±0.16</b>	<b>94.22±0.10</b>	<b>86.59±0.14</b>	<b>64.47±0.15</b>	<b>67.51±0.18</b>
ROC	Recall	BiRD [14]	34.76±0.11	61.79±0.15	53.74±0.14	-	60.40±0.17	96.61±0.18	-	84.65±0.12	65.33±0.14
		BiRD [14] + RoPE-Mixed [12]	39.78±0.13	62.13±0.19	74.27±0.11	-	61.33±0.13	96.61±0.17	-	84.65±0.15	69.80±0.12
		BiRD [14] + MCG-RoPE (Ours)	44.47±0.15	64.20±0.18	83.75±0.11	-	62.19±0.14	96.61±0.19	-	85.22±0.16	72.74±0.13
		BiRD [14] + $V_k D$ [30]	53.19±0.17	69.10±0.14	90.84±0.19	-	61.71±0.10	<b>100±0.00</b>	-	81.15±0.12	76.00±0.15
		BiRD [14] + Pseudo-KD (Ours)	58.47±0.16	69.92±0.12	95.83±0.18	-	66.32±0.11	<b>100±0.00</b>	-	86.58±0.13	79.52±0.14
		ClinKD (Ours)	<b>61.42±0.17</b>	<b>71.30±0.19</b>	<b>97.00±0.18</b>	-	<b>68.84±0.12</b>	<b>100±0.00</b>	-	<b>95.54±0.11</b>	<b>82.35±0.15</b>
RC	SPICE [2]	BiRD [14]	41.88±0.12	51.69±0.14	37.39±0.18	47.95±0.15	54.07±0.10	77.44±0.16	48.73±0.13	82.65±0.19	55.23±0.14
		BiRD [14] + RoPE-Mixed [12]	43.51±0.15	51.88±0.18	54.61±0.13	52.83±0.19	54.07±0.11	68.15±0.17	53.99±0.12	65.28±0.14	55.54±0.13
		BiRD [14] + MCG-RoPE (Ours)	50.73±0.14	53.11±0.16	60.33±0.12	70.16±0.18	54.07±0.11	70.18±0.19	61.52±0.15	70.46±0.17	61.32±0.13
		BiRD [14] + $V_k D$ [30]	51.33±0.13	54.39±0.17	62.83±0.19	74.31±0.14	54.07±0.15	76.23±0.12	67.89±0.18	72.15±0.11	64.15±0.16
		BiRD [14] + Pseudo-KD (Ours)	52.78±0.12	58.41±0.15	70.39±0.18	75.85±0.13	<b>55.22±0.16</b>	81.34±0.11	71.54±0.17	72.15±0.14	67.21±0.19
		ClinKD (Ours)	<b>53.94±0.14</b>	<b>58.41±0.12</b>	<b>71.47±0.18</b>	<b>79.91±0.15</b>	52.10±0.11	<b>83.92±0.19</b>	<b>84.51±0.13</b>	<b>80.19±0.16</b>	<b>70.56±0.17</b>
MIA	mBMR [14]	BiRD [14]	47.01±0.14	49.35±0.18	37.17±0.15	57.15±0.12	39.91±0.17	72.13±0.13	48.87±0.16	65.78±0.19	52.17±0.11
		BiRD [14] + RoPE-Mixed [12]	57.10±0.17	50.89±0.13	42.55±0.16	69.28±0.11	41.63±0.18	73.32±0.14	59.63±0.15	61.80±0.10	57.03±0.19
		BiRD [14] + MCG-RoPE (Ours)	60.53±0.16	53.77±0.11	54.10±0.18	62.01±0.12	43.88±0.15	75.33±0.14	62.89±0.19	64.53±0.13	59.63±0.17
		BiRD [14] + $V_k D$ [30]	62.33±0.10	53.77±0.15	52.27±0.19	62.01±0.16	47.29±0.13	75.33±0.17	68.04±0.12	70.31±0.18	61.42±0.14
		BiRD [14] + Pseudo-KD (Ours)	66.85±0.11	55.73±0.14	52.27±0.17	64.74±0.15	<b>50.58±0.12</b>	78.21±0.19	70.02±0.13	<b>76.16±0.18</b>	64.32±0.16
		ClinKD (Ours)	<b>66.85±0.13</b>	<b>56.82±0.16</b>	<b>54.01±0.18</b>	<b>67.08±0.14</b>	<b>50.58±0.11</b>	<b>81.00±0.15</b>	<b>70.02±0.17</b>	76.05±0.19	<b>65.69±0.12</b>
Average	-	BiRD [14]	43.03±0.12	48.02±0.11	42.51±0.17	53.85±0.19	51.99±0.14	80.45±0.16	60.58±0.13	69.78±0.15	-
		BiRD [14] + RoPE-Mixed [12]	46.82±0.17	54.50±0.12	53.37±0.15	60.98±0.13	52.63±0.18	79.08±0.10	66.26±0.19	66.14±0.11	-
		BiRD [14] + MCG-RoPE (Ours)	51.74±0.13	55.12±0.19	61.03±0.12	66.92±0.17	55.13±0.14	82.60±0.15	70.33±0.11	70.52±0.18	-
		BiRD [14] + $V_k D$ [30]	56.41±0.16	57.05±0.11	62.91±0.19	67.40±0.14	55.18±0.18	86.22±0.10	71.73±0.15	70.88±0.13	-
		BiRD [14] + Pseudo-KD (Ours)	60.17±0.14	59.23±0.16	66.42±0.12	68.96±0.19	<b>57.99±0.13</b>	88.31±0.15	76.66±0.17	74.44±0.10	-
		ClinKD (Ours)	<b>61.93±0.15</b>	<b>59.69±0.18</b>	<b>67.76±0.19</b>	<b>72.08±0.13</b>	57.97±0.16	<b>89.79±0.11</b>	<b>80.37±0.14</b>	<b>79.06±0.12</b>	-

Table 3. Comparison with other SOTA methods on Med-GRIT-Test30k [7, 39]. We evaluate the performance on eight modalities.

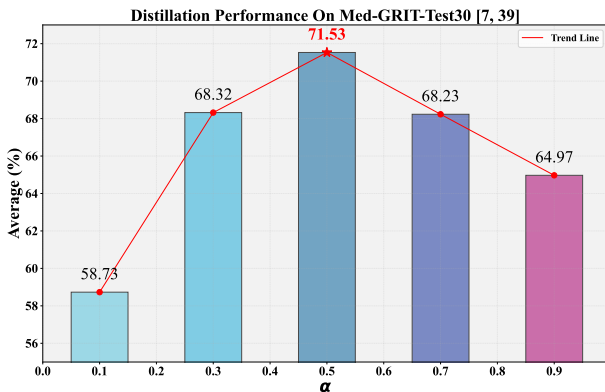


Figure 4. Effect of value of  $\alpha$  in Pseudo-Labels Medical Knowledge Distillation.

qa0.2k [46]. LLaVA-Med [18] still achieves the best performance. Although ClinKD has not yet surpassed LLaVA-Med [18] on this dataset, it still achieved a 2.69% improvement over BiRD [14] in the MIA task. The limitation may be caused by the different sources of medical data so that the ClinKD may fail to leverage medical knowledge to analyze medical images.

#### 4.4.2. Ablation study

**Effect of Qwen2-VL [34].** Table 2 presents the ablation study of proposed methods. To investigate the impact of model upgrade on the experiment, we applied the same training strategy to Qwen2-VL as we did to BiRD [14]. The results show that the model upgrade only has a significant effect on the MIA task, which shows Qwen2-VL [34] out-

performs BiRD by 10.06%.

**Effect of Med-CLIP Guided Rotary Position Embedding.** As shown in Table 2, with adding MCG-RoPE to BiRD, all metrics exhibit significant enhancements, with the average rising from 56.66% to 64.44%. This indicates the importance of adequate image-text alignment.

**Effect of Pseudo-Labels Medical Knowledge Distillation.** Table 2 represents improvements achieved by using Pseudo-Labels Medical Knowledge Distillation that leads to enhancements by 12.41%, 14.19%, 11.98% and 12.15% in the VG, ROC, RC and MIA tasks, respectively. The results illustrate that providing prior medical knowledge by using Pseudo-Labels Medical Knowledge Distillation can fill MLLMs’ gap of medical knowledge, boosting capabilities of adapting to new medical knowledge.

Figure 4 shows the effect of different values of  $\alpha$  in Eq. (16). In this experiment, the average performance achieves the best when we set  $\alpha = 0.5$ . Both excessively high and low alpha values can lead to performance degradation. This might be because a low  $\alpha$  value prevents ClinKD from learning sufficient prior medical knowledge, while an overly high alpha value tends to make ClinKD generate irrational pseudo-labels that contradict common medical knowledge.

**Effect of Semantic-Aware Selective Generation.** From the results in Table 2, we can see a light enhancement on VG and ROC task. However, there is a slight decrease in the metric scores on the RC and MIA tasks. These results may be caused by the semantic similarity from CLIP models that are affected by complex sentences.

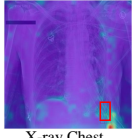
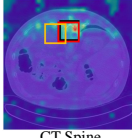

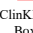
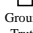

Visualization of Attention	Ground Caption Task	Visual Grounding Task
		
		
		
		
Questions	Can you describe the characteristics of the object at <code>&lt;box_start&gt;(772,833),(856,983)&lt;box_end&gt;?</code>	Where is the vertebrae T11 located in the image?
BiRD [14] (SOTA)	The object shows indications of edema, which is the presence of air in the pleural space causing lung collapse.	The <code>&lt;object_ref_start&gt;</code> vertebrae T11 <code>&lt;object_ref_end&gt;</code> is located at the coordinates <code>&lt;box_start&gt;(331,194),(482,324)&lt;box_end&gt;</code> .
ClinKD (Ours)	The object shows indications of pneumothorax, which is the presence of air in the pleural space causing lung collapse.	The <code>&lt;object_ref_start&gt;</code> vertebrae T11 <code>&lt;object_ref_end&gt;</code> is located at the coordinates <code>&lt;box_start&gt;(433,166),(578,314)&lt;box_end&gt;</code> .
Ground Truth	The object shows indications of pneumothorax, which is the presence of air in the pleural space causing lung collapse.	The <code>&lt;object_ref_start&gt;</code> vertebrae T11 <code>&lt;object_ref_end&gt;</code> is located at the coordinates <code>&lt;box_start&gt;(423,177),(578,320)&lt;box_end&gt;</code> .

Figure 5. Visualization of attentions on GC and VG tasks. The ClinKD generates better answers compared with BiRD [14].

#### 4.4.3. Comparison with Other Methods

**Comparison with BiRD + RoPE-Mixed [12].** The RoPE-Mixed uses frequencies for both axes as learnable network parameters, effectively handling image features in diagonal direction. It achieves the best performance in different visual scenarios [23, 48, 49]. Hence we compare our MCG-RoPE with RoPE-Mixed. As shown in Table 3, by adding RoPE-Mixed to BiRD [14], great achievements take place on all modalities (CT, MR, X-ray, etc.). Compared with RoPE-Mixed [12], our MCG-RoPE outperforms it by 4.95%, 2.94%, 5.78% and 2.60% on VG, ROC, RC and MIA tasks, respectively. For more detailed performance on the 8 modalities, MCG-RoPE still achieves the best improvements most of the time.

**Comparison with BiRD +  $V_kD$  [30].**  $V_kD$  is a novel method that can improve knowledge distillation. This work utilizes a projection layer for maximizing the knowledge transfer to the student backbone. Many experiments [8, 13, 31, 33] have been made to prove the best performance of this method. Compared with BiRD with  $V_kD$  in the Table 3, Pseudo-KD shows its advantages on multi-task fine-grained Med-VQA scenarios, outperforming  $V_kD$  almost on all modalities.

#### 4.4.4. Case Study

**Case study on Med-GRIT-Test30 [7, 39].** Figure 5 illustrates the visualization of the attention map and a comparison among BiRD [14], ClinKD (ours), and the ground truth. The grounding of ClinKD is more accurate because MCG-RoPE can improve image-text alignment, and at the same time, Pseudo-KD enables ClinKD to better adapt to medical knowledge.

**Case study on Additional VQA-RAD [16].** As shown in Figure 6, we conducted an experiment on VQA-RAD [16]. Despite the relatively simple annotations, ClinKD pro-

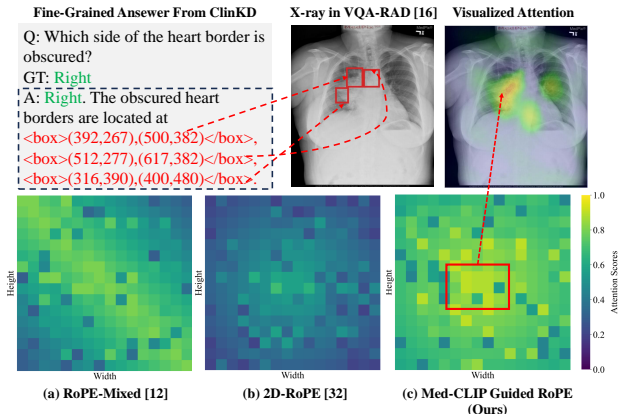


Figure 6. An example from VQA-RAD [16] and the performance of RoPE variants.

vides fine-grained answers with three accurate groundings, demonstrating its precision in response.

To assess the models' attention to pathological features, we conducted a comparative analysis of three RoPE variants. The results indicate that 2D-RoPE [32] tends to show low attention on pathological regions. In contrast, RoPE-Mixed [12] demonstrates a greater emphasis on diagonal features. Notably, our Med-CLIP Guided RoPE specifically targets and enhances the model's attention to pathological regions, thereby facilitating more accurate alignment between text and images, especially in the identification of relevant medical features.

#### 4.4.5. Limitation

Although our method alleviates, to some extent, the issue of insufficient prior knowledge and achieves impressive state-of-the-art performance on the Med-GRIT-270k [7, 39] dataset, the model still exhibits hallucinations. Furthermore, through comparative evaluations on the LLaVA-Med-qa0.2k [46] dataset, our approach remains insufficient to enable the model to emerge with strong generalization capabilities in Med-VQA domain. Creating high-quality Med-VQA datasets and training medical prior knowledge before freezing the visual encoder could significantly enhance the model's generalization ability on medical data.

## 5. Conclusion

In this work, we propose ClinKD, a novel medical distiller centered on Pseudo-Labels Medical Knowledge Distillation and Reflective Correction Training. In addition, we propose the Med-CLIP Guided RoPE to improve image-text alignment. They are designed to enhance the performance on fine-grained multi-task datasets in Med-VQA domain. Extensive experiments demonstrate that our Med-CLIP Guided RoPE achieves superior image-text alignment, while the Pseudo-Labels Medical Knowledge Distillation effectively bridges prior medical knowledge gaps.



These mechanisms synergistically enhance the model’s medical knowledge adaptation capabilities.

In future work, further refinements to the distillation process, along with the incorporation of more comprehensive medical knowledge and higher-quality datasets, could significantly improve model’s robustness and reduce the model’s reliance on manually labeled data.

## 6. Acknowledgments

This work was supported by the Natural Science Foundation of Guangdong Province (No. 2023A1515010673), in part by the Shenzhen Science and Technology Innovation Bureau key project (No. JSGG20220831110400001, No. CJGJZD20230724093303007, KJZD20240903101259001), in part by Shenzhen Medical Research Fund (No. D2404001), in part by Shenzhen Engineering Laboratory for Diagnosis & Treatment Key Technologies of Interventional Surgical Robots (XMHT20220104009), and the Key Laboratory of Biomedical Imaging Science and System, CAS, for the Research platform support.

## References

- [1] Asma Ben Abacha, Sadid A. Hasan, Vivek Datla, Joey Liu, Dina Demner-Fushman, and Henning Müller. Vqa-med: Overview of the medical visual question answering task at imageclef 2019. In *Conference and Labs of the Evaluation Forum*, 2019. 1
- [2] Peter Anderson, Basura Fernando, Mark Johnson, and Stephen Gould. Spice: Semantic propositional image caption evaluation. In *Computer Vision – ECCV 2016*, pages 382–398, Cham, 2016. Springer International Publishing. 6, 7
- [3] Jinze Bai, Shuai Bai, Shusheng Yang, Shijie Wang, Sinan Tan, Peng Wang, Junyang Lin, Chang Zhou, and Jingren Zhou. Qwen-vl: A versatile vision-language model for understanding, localization, text reading, and beyond. *arXiv preprint arXiv:2308.12966*, 1(8), 2023. 3
- [4] Davide Caffagni, Federico Cocchi, Luca Barsellotti, Nicholas Moratelli, Sara Sarto, Lorenzo Baraldi, Lorenzo Baraldi, Marcella Cornia, and Rita Cucchiara. The revolution of multimodal large language models: A survey. In *Findings of the Association for Computational Linguistics: ACL 2024*, pages 13590–13618, Bangkok, Thailand, 2024. Association for Computational Linguistics. 1
- [5] Xupeng Chen, Zhixin Lai, Kangrui Ruan, Shichu Chen, Jiayang Liu, and Zuozhu Liu. R-llava: Improving med-vqa understanding through visual region of interest. *arXiv preprint arXiv:2410.20327*, 2024. 1
- [6] Zeming Chen, Wenwei Zhang, Xinjiang Wang, Kai Chen, and Zhi Wang. Mixed pseudo labels for semi-supervised object detection. *arXiv preprint arXiv:2312.07006*, 2023. 2
- [7] Junlong Cheng, Jin Ye, Zhongying Deng, Jianpin Chen, Tianbin Li, Haoyu Wang, Yanzhou Su, Ziyang Huang, Jilong Chen, Lei Jiang, et al. Sam-med2d. *arXiv preprint arXiv:2308.16184*, 2023. 6, 7, 8
- [8] Kaiwen Cui, Yingchen Yu, Fangneng Zhan, Shengcai Liao, Shijian Lu, and Eric P. Xing. Kd-dlgn: Data limited image generation via knowledge distillation. In *Proceedings of the IEEE/CVF Conference on Computer Vision and Pattern Recognition (CVPR)*, pages 3872–3882, 2023. 8
- [9] Xiaotang Gai, Chenyi Zhou, Jiayang Liu, YANG FENG, Jian Wu, and Zuozhu Liu. Enhancing medical VQA with multimodal determination rationales. In *GenAI for Health: Potential, Trust and Policy Compliance*, 2024. 1
- [10] Sadid A. Hasan, Yuan Ling, Oladimeji Farri, Joey Liu, Henning Müller, and Matthew P. Lungren. Overview of imageclef 2018 medical domain visual question answering task. In *Conference and Labs of the Evaluation Forum*, 2018. 1
- [11] Jinlong He, Pengfei Li, Gang Liu, and Shenjun Zhong. Parameter-efficient fine-tuning medical multimodal large language models for medical visual grounding. *arXiv preprint arXiv:2410.23822*, 2024. 1
- [12] Byeongho Heo, Song Park, Dongyoon Han, and Sangdoon Yun. Rotary position embedding for vision transformer. In *Computer Vision – ECCV 2024*, pages 289–305, Cham, 2025. Springer Nature Switzerland. 3, 7, 8
- [13] Geoffrey Hinton, Oriol Vinyals, and Jeff Dean. Distilling the knowledge in a neural network. *arXiv preprint arXiv:1503.02531*, 2015. 8
- [14] Xiaoshuang Huang, Haifeng Huang, Lingdong Shen, Yehui Yang, Fangxin Shang, Junwei Liu, and Jia Liu. A refer-and-ground multimodal large language model for biomedicine. In *Medical Image Computing and Computer Assisted Intervention – MICCAI 2024*, pages 399–409, Cham, 2024. Springer Nature Switzerland. 1, 2, 3, 5, 6, 7, 8
- [15] Gurucharan Marthi Krishna Kumar, Aman Chadha, Janine Mendola, and Amir Shmuel. Medvisionllama: Leveraging pre-trained large language model layers to enhance medical image segmentation. *arXiv preprint arXiv:2410.02458*, 2024. 1
- [16] Jason J Lau, Soumya Gayen, Asma Ben Abacha, and Dina Demner-Fushman. A dataset of clinically generated visual questions and answers about radiology images. *Scientific data*, 5(1):1–10, 2018. 2, 8
- [17] Chen Li, Yixiao Ge, Dian Li, and Ying Shan. Vision-language instruction tuning: A review and analysis. *arXiv preprint arXiv:2311.08172*, 2023. 2
- [18] Chunyuan Li, Cliff Wong, Sheng Zhang, Naoto Usuyama, Haotian Liu, Jianwei Yang, Tristan Naumann, Hoifung Poon, and Jianfeng Gao. Llava-med: Training a large language-and-vision assistant for biomedicine in one day. *Advances in Neural Information Processing Systems*, 36:28541–28564, 2023. 1, 2, 3, 6, 7
- [19] Shutao Li, Bin Li, Bin Sun, and Yixuan Weng. Towards visual-prompt temporal answer grounding in instructional video. *IEEE Transactions on Pattern Analysis and Machine Intelligence*, 2024. 1
- [20] Yundong Li, Longxia Guo, and Yizheng Ge. Pseudo labels for unsupervised domain adaptation: A review. *Electronics*, 12(15), 2023. 2
- [21] Chia Xin Liang, Pu Tian, Caitlyn Heqi Yin, Yao Yua, Wei An-Hou, Li Ming, Tianyang Wang, Ziqian Bi, and Ming

- Liu. A comprehensive survey and guide to multimodal large language models in vision-language tasks. *arXiv preprint arXiv:2411.06284*, 2024. 1
- [22] Xinjie Liang, Xiangyu Li, Fanding Li, Jie Jiang, Qing Dong, Wei Wang, Kuanquan Wang, Suyu Dong, Gongning Luo, and Shuo Li. Medfilip: Medical fine-grained language-image pre-training. *IEEE Journal of Biomedical and Health Informatics*, pages 1–11, 2025. 2
- [23] Tsung Yi Lin, Michael Maire, Serge Belongie, James Hays, Pietro Perona, Deva Ramanan, Piotr Dollár, and C. Lawrence Zitnick. Microsoft coco: Common objects in context. In *Lecture Notes in Computer Science, Springer*, pages 740–755. Springer, 2014. 13th European Conference on Computer Vision, ECCV 2014 ; Conference date: 06-09-2014 Through 12-09-2014. 8
- [24] Tianwei Lin, Wenqiao Zhang, Sijing Li, Yuqian Yuan, Binhe Yu, Haoyuan Li, Wangui He, Hao Jiang, Mengze Li, Xiaohui Song, et al. Healthgpt: A medical large vision-language model for unifying comprehension and generation via heterogeneous knowledge adaptation. *arXiv preprint arXiv:2502.09838*, 2025. 2
- [25] Zhihong Lin, Donghao Zhang, Qingyi Tao, Danli Shi, Ghulamreza Haffari, Qi Wu, Mingguang He, and Zongyuan Ge. Medical visual question answering: A survey. *Artificial Intelligence in Medicine*, 143:102611, 2023. 1
- [26] Bo Liu, Li-Ming Zhan, Li Xu, Lin Ma, Yan Yang, and Xiao-Ming Wu. Slake: A semantically-labeled knowledge-enhanced dataset for medical visual question answering. In *2021 IEEE 18th International Symposium on Biomedical Imaging (ISBI)*, pages 1650–1654. IEEE, 2021. 2
- [27] Haotian Liu, Chunyuan Li, Qingyang Wu, and Yong Jae Lee. Visual instruction tuning. In *Advances in Neural Information Processing Systems*, pages 34892–34916. Curran Associates, Inc., 2023. 1, 2
- [28] Haotian Liu, Chunyuan Li, Yuheng Li, and Yong Jae Lee. Improved baselines with visual instruction tuning. In *Proceedings of the IEEE/CVF Conference on Computer Vision and Pattern Recognition (CVPR)*, pages 26296–26306, 2024. 2
- [29] Tengfei Liu, Jiapu Wang, Yongli Hu, Mingjie Li, Junfei Yi, Xiaojun Chang, Junbin Gao, and Baocai Yin. Hc-llm: Historical-constrained large language models for radiology report generation. *arXiv preprint arXiv:2412.11070*, 2024. 1
- [30] Roy Miles, Ismail Elezi, and Jiankang Deng. Vkd: Improving knowledge distillation using orthogonal projections. In *Proceedings of the IEEE/CVF Conference on Computer Vision and Pattern Recognition (CVPR)*, pages 15720–15730, 2024. 7, 8
- [31] Nikolaos Passalis and Anastasios Tefas. Learning deep representations with probabilistic knowledge transfer. In *Proceedings of the European Conference on Computer Vision (ECCV)*, 2018. 8
- [32] Jianlin Su, Murtadha Ahmed, Yu Lu, Shengfeng Pan, Wen Bo, and Yunfeng Liu. Roformer: Enhanced transformer with rotary position embedding. *Neurocomputing*, 568:127063, 2024. 1, 2, 3, 8
- [33] Frederick Tung and Greg Mori. Similarity-preserving knowledge distillation. In *Proceedings of the IEEE/CVF International Conference on Computer Vision (ICCV)*, 2019. 8
- [34] Peng Wang, Shuai Bai, Sinan Tan, Shijie Wang, Zhihao Fan, Jinze Bai, Keqin Chen, Xuejing Liu, Jialin Wang, Wenbin Ge, et al. Qwen2-vl: Enhancing vision-language model’s perception of the world at any resolution. *arXiv preprint arXiv:2409.12191*, 2024. 6, 7
- [35] Xinyu Wang, Min Gui, Yong Jiang, Zixia Jia, Nguyen Bach, Tao Wang, Zhongqiang Huang, and Kewei Tu. ITA: Image-text alignments for multi-modal named entity recognition. In *Proceedings of the 2022 Conference of the North American Chapter of the Association for Computational Linguistics: Human Language Technologies*, pages 3176–3189, Seattle, United States, 2022. Association for Computational Linguistics. 2
- [36] Xilin Wei, Xiaoran Liu, Yuhang Zang, Xiaoyi Dong, Pan Zhang, Yuhang Cao, Jian Tong, Haodong Duan, Qipeng Guo, Jiaqi Wang, et al. Videorope: What makes for good video rotary position embedding? *arXiv preprint arXiv:2502.05173*, 2025. 3
- [37] Enneng Yang, Li Shen, Guibing Guo, Xingwei Wang, Xiaochun Cao, Jie Zhang, and Dacheng Tao. Model merging in llms, mllms, and beyond: Methods, theories, applications and opportunities. *arXiv preprint arXiv:2408.07666*, 2024. 1
- [38] Hang Yang, Hao Chen, Hui Guo, Yineng Chen, Ching-Sheng Lin, Shu Hu, Jinrong Hu, Xi Wu, and Xin Wang. Llm-medqa: Enhancing medical question answering through case studies in large language models. *arXiv preprint arXiv:2501.05464*, 2024. 1
- [39] Jin Ye, Junlong Cheng, Jianpin Chen, Zhongying Deng, Tianbin Li, Haoyu Wang, Yanzhou Su, Ziyang Huang, Jilong Chen, Lei Jiang, et al. Sa-med2d-20m dataset: Segment anything in 2d medical imaging with 20 million masks. *arXiv preprint arXiv:2311.11969*, 2023. 6, 7, 8
- [40] Haoxuan You, Haotian Zhang, Zhe Gan, Xianzhi Du, Bowen Zhang, Zirui Wang, Liangliang Cao, Shih-Fu Chang, and Yinfei Yang. Ferret: Refer and ground anything anywhere at any granularity. *arXiv preprint arXiv:2310.07704*, 2023. 2
- [41] Zhen Zeng, Leijiang Gu, Xun Yang, Zhangling Duan, Zenglin Shi, and Meng Wang. Visual-oriented fine-grained knowledge editing for multimodal large language models. *arXiv preprint arXiv:2411.12790*, 2024. 2
- [42] Haotian Zhang, Haoxuan You, Philipp Dufter, Bowen Zhang, Chen Chen, Hong-You Chen, Tsu-Jui Fu, William Yang Wang, Shih-Fu Chang, Zhe Gan, et al. Ferret-v2: An improved baseline for referring and grounding with large language models. *arXiv preprint arXiv:2404.07973*, 2024. 2
- [43] Kun Zhang, Zhendong Mao, Quan Wang, and Yongdong Zhang. Negative-aware attention framework for image-text matching. In *2022 IEEE/CVF Conference on Computer Vision and Pattern Recognition (CVPR)*, pages 15640–15649, 2022. 2
- [44] Kai Zhang, Rong Zhou, Eashan Adhikarla, Zhiling Yan, Yixin Liu, Jun Yu, Zhengliang Liu, Xun Chen, Brian D.

- Davison, Hui Ren, Jing Huang, Chen Chen, Yuyin Zhou, Sunyang Fu, Wei Liu, Tianming Liu, Xiang Li, Yong Chen, Lifang He, James Zou, Quanzheng Li, Hongfang Liu, and Lichao Sun. A generalist vision–language foundation model for diverse biomedical tasks. *Nature Medicine*, 30(11): 3129–3141, 2024. [2](#)
- [45] Shengyu Zhang, Linfeng Dong, Xiaoya Li, Sen Zhang, Xiaofei Sun, Shuhe Wang, Jiwei Li, Runyi Hu, Tianwei Zhang, Fei Wu, et al. Instruction tuning for large language models: A survey. *arXiv preprint arXiv:2308.10792*, 2023. [2](#)
- [46] Sheng Zhang, Yanbo Xu, Naoto Usuyama, Hanwen Xu, Jaspreet Bagga, Robert Tinn, Sam Preston, Rajesh Rao, Mu Wei, Naveen Valluri, et al. Biomedclip: a multimodal biomedical foundation model pretrained from fifteen million scientific image-text pairs. *arXiv preprint arXiv:2303.00915*, 2023. [2](#), [6](#), [7](#), [8](#)
- [47] Yumin Zhang, Hongliu Li, Yawen Hou, Xiuyi Chen, Hongyuan Yu, and Long Xia. Consecutive knowledge meta-adaptation learning for unsupervised medical diagnosis. *Knowledge-Based Systems*, 291:111573, 2024. [2](#)
- [48] Bolei Zhou, Hang Zhao, Xavier Puig, Sanja Fidler, Adela Barriuso, and Antonio Torralba. Scene parsing through ade20k dataset. In *2017 IEEE Conference on Computer Vision and Pattern Recognition (CVPR)*, pages 5122–5130, 2017. [8](#)
- [49] Bolei Zhou, Hang Zhao, Xavier Puig, Tete Xiao, Sanja Fidler, Adela Barriuso, and Antonio Torralba. Semantic understanding of scenes through the ade20k dataset. *International Journal of Computer Vision*, 127:302–321, 2019. [8](#)